Microfluid Nanofluid (2017) 21:176
https://doi.org/10.1007/s10404-017-2012-6

RESEARCH PAPER

Piezo-driven acoustic streaming in an electrowetting-on-dielectric digital microfluidics device

Andrew C. Madison[1] · Mathew W. Royal[1] · Richard B. Fair[1]

Received: 26 June 2017 / Accepted: 1 November 2017 / Published online: 10 November 2017

Abstract We report the integration of a lead zirconate titanate, $Pb[Zr_xTi_{1-x}O_3]$ (PZT), piezoelectric transducer disk into the top plate of an otherwise conventional electrowetting-on-dielectric (EWD) digital microfluidics device to demonstrate on-demand induction of circulating fluid flow within single 200 nL droplets. Microparticle image velocimetry was used to measure in-plane velocity distributions for PZT excitation voltages that ranged from 0 to 50 V_{RMS}. Intra-droplet streaming velocities in excess of 2.0 mm · s^{-1} were observed without droplet breakup or damage to the EWD device layer. Additionally, we found median intra-droplet streaming velocity to depend quadratically on PZT excitation voltage up to the stress limit of the interfacial boundary. Our approach offers an alternative device architecture for active micromixing strategies in EWD digital microfluidics laboratory-on-chip systems.

Keywords Electrowetting on dielectric · Digital microfluidics · Acoustofluidics · Acoustic streaming · Piezoelectric transducer · Particle image velocimetry

DARPA Grant HR0011-12-C-0057.

Electronic supplementary material The online version of this article (https://doi.org/10.1007/s10404-017-2012-6) contains supplementary material, which is available to authorized users.

✉ Andrew C. Madison
andrew.c.madison@ieee.org

Mathew W. Royal
matthew.w.royal@gmail.com

Richard B. Fair
rfair@duke.edu

[1] Department of Electrical and Computer Engineering, Duke University, 130 Hudson Hall, Box 90291, Durham, NC, USA

1 Introduction

As electrowetting-on-dielectric (EWD) digital microfluidic systems mature beyond the realm of research, EWD applications are gaining traction in commercial laboratory-on-chip (LoC) applications (Illumina 2016; eplex 2016). Despite this progress, long mixing times, due to the laminar flow regime in which these devices operate, persist as a problem for LoC assay development. In the EWD environment, active mixing is typically carried out by intra-droplet hydrodynamic flows generated during transport operations among neighboring electrodes (Lu et al. 2008) or in stationary droplets perturbed by rapid actuator oscillation (Mugele et al. 2006; Baret et al. 2007; Ko et al. 2008; Lee 2010). Although these methods are many times faster than diffusion alone, EWD-based mixing is limited by the response time of the droplet and may require frequency tuning to resonantly drive droplet oscillations that ultimately yield complete homogenization (Ko et al. 2008; Lee 2010). While others have sought to achieve active micromixing through the integration of piezoelectric materials onto the EWD bottom plate, which complicates EWD device fabrication and limits choices of EWD substrates to piezoelectric materials, we introduce the use of a piezoelectric transducer assembled into the top plate of a parallel-plate EWD device to generate intra-droplet circulating flows in stationary droplets with ultrasound-induced acoustic streaming (Li et al. 2012). With a simple modification to conventional fabrication methods, our approach liberates the design space of piezoelectrically enabled EWD devices from the material constraint imposed by bottom plate integration. Additionally, the integration methodology discussed herein offers flexibility in terms of transducer selection and placement, which directly impacts the implementation of ultrasound-mediated LoC applications.

The EWD phenomenon involves modulation of the wetting behavior of a polarizable liquid droplet on a hydrophobic, insulated electrode by an applied electric field (Lippmann 1875; Berge 1993). The Young–Lippmann equation (Eq. 1) is frequently used to approximate the mechanism of EWD actuation:

$$\cos\theta = \cos\theta_0 + \frac{\varepsilon_0\varepsilon_r V^2}{2d\gamma_{LV}} = \cos\theta_0 + \eta, \tag{1}$$

where θ is the voltage-dependent electrowetting contact angle, θ_0 is Young's angle of the system at zero voltage, d is the thickness of the dielectric with permittivity, $\varepsilon_0\varepsilon_r$, γ_{LV} is the interfacial tension between the droplet and the surrounding medium, and η is the electrowetting number. The wetting behavior captured in the Young–Lippmann model arises from the generation of a localized electrowetting force that counteracts surface tension forces acting at a fluid interface and reduces the macroscopic contact angle of the droplet, θ (Lippmann 1875; Pollack et al. 2002; Mugele et al. 2006; Mugele 2009). As shown in Eq. 2, the electrowetting force is proportional to the square of the applied voltage, V, and is oriented normal to the droplet interface, $\hat{\mathbf{n}}$, at the contact line.

$$\mathbf{f}_{EWD} = \frac{\varepsilon_0\varepsilon_r V^2}{2d}\hat{\mathbf{n}}. \tag{2}$$

During actuation the electrowetting force acts on lengths of the contact line exposed to energized electrodes, effectively pulling the droplet toward regions of greater wettability. As a droplet settles on an activated electrode, the symmetry shared between the contact line of the droplet and the actuator geometry results in axially symmetric electrowetting forces that stabilize the droplet in place. Thus, the electrowetting force can be exploited as a means of driving droplet transport or, in the present case, as an immobilization force that resists an external acoustic perturbation of the fluid interface.

In general, acoustofluidic micromixers rely on mechanical couplings between a fluid volume and piezoelectric devices or materials to enhance fluid mixing through the induction of fluid flow. Oscillating sidewall microstructures (Huang et al. 2013) or trapped bubbles (Liu et al. 2002; Ahmed et al. 2009), excitation of resonance modes in microfluidic channels (Bruus 2011, 2012), and propagating shear waves (Shilton et al. 2008; Luong et al. 2011; Alghane et al. 2012) represent the most common demonstrations of acoustofluidic micromixers. While many studies focus on generating flows in continuous-flow microfluidic devices, few address the challenge of coupling ultrasound to single droplets in EWD devices. One such study reports enhanced intra-droplet mixing by acoustic excitation of interdigitated lithium niobate ($LiNBO_3$) microstructures for generating surface acoustic waves (SAW) near an immobilized droplet (Li et al. 2012). While elegant and effective, integration of exotic piezoelectric films onto an EWD substrate may not always be an option for device fabrication. In seeking a simpler approach, we investigated the integration of a piezoelectric ultrasound transducer into the EWD top plate for application of localized acoustic perturbation within an EWD-immobilized droplet. In contrast to the SAW approach, which exploits in-plane mechanical shear waves to drive intra-droplet fluid flow, the present work exploits a thin (5 mil, 127 μm) planarizing film to couple ultrasonic PZT oscillations directly into a 200-nL droplet held in place by EWD actuation.

Pioneered by Rayleigh (1884) and Eckart (1948), acoustic streaming is a steady fluid flow formed by viscous attenuation of an acoustic wave (Riley 2001; Wiklund et al. 2012). As an acoustic wave propagates through a fluid, the amplitude of the wave attenuates and, in doing so, drives a nonzero net displacement of fluid during each oscillation. Over many cycles, the net displacement is observed as a steady time-averaged momentum transfer into the fluid (Wiklund et al. 2012). Acoustic streaming fluid velocities obey the time-averaged continuity equation and Navier–Stokes equation, shown in Eqs. (3) and (4), respectively (Muller et al. 2012).

$$\rho_0\nabla\cdot\langle\mathbf{v}_2\rangle = -\nabla\cdot\langle\rho_1\mathbf{v}_1\rangle \tag{3}$$

$$\langle\rho_1\frac{\partial\mathbf{v}_1}{\partial t}\rangle + \rho_0\langle(\mathbf{v}_1\cdot\nabla)\mathbf{v}_1\rangle = \mu\nabla^2\langle\mathbf{v}_2\rangle + \beta\mu\nabla(\nabla\cdot\langle\mathbf{v}_2\rangle) - \nabla\langle p_2\rangle, \tag{4}$$

where the time average over a full period of oscillation, T, is denoted by the angled brackets, $\langle\ldots\rangle = \frac{1}{T}\int_{t_0}^{t_0+T}\ldots dt$; the pressure, p, density, ρ, and velocity, v, fields result from summations over respective zeroth-, first-, and second-order terms: $p = p_0 + p_1 + p_2$, $\rho = \rho_0 + \rho_1$, and $\mathbf{v} = \mathbf{v}_1 + \mathbf{v}_2$; μ is dynamic viscosity; and β is the viscosity ratio, which is typically $\frac{1}{3}$ for simple fluids (Muller et al. 2012). In most cases, a single moving boundary, $\partial\Omega$, drives the system with harmonic oscillation of the form: $\mathbf{v}_1(t)|_{\mathbf{x}=\partial\Omega} = \mathbf{v}_b e^{-i\omega t}$, where $\mathbf{v}_b$ is the velocity of the boundary, the angular frequency of the oscillation is given by $\omega = 2\pi f$, and t is time.

The present work leverages a lead zirconate titanate (PZT) piezoelectric transducer disk to expose aqueous single droplets and a surrounding silicone oil filler fluid to bursts of ultrasound energy that drive second-order acoustic streaming velocities in the droplet vicinity. The objective of this study was threefold: (1) to demonstrate the simple assembly of a PZT-enabled EWD device with a thin coupling film; (2) to identify experimental parameters for generating acoustic streaming flows within EWD-immobilized droplets; and (3)

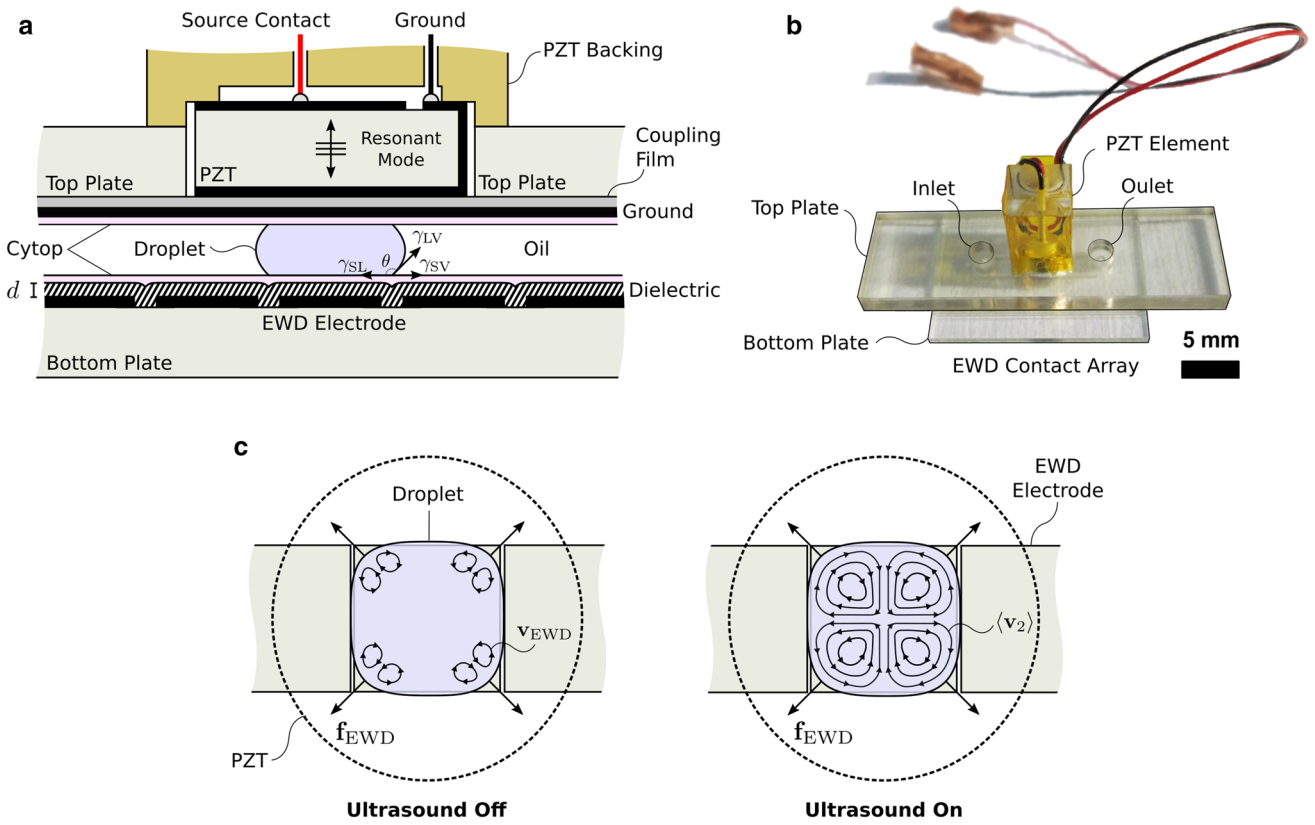

Fig. 1 Schematic, device, and concept of the integration of a piezoelectric component into an electrowetting-on-dielectric digital microfluidic device for intra-droplet acoustic streaming. **a** Device schematic (not drawn to scale). **b** Assembled test device. **c** Approximate flow fields observed in the absence (left) and presence (right) of 250 kHz ultrasound perturbation

to characterize the induced flow fields using fluorescence microscopy and particle image velocimetry.

The accessibility of the acoustic coupling method presented in this work provides a viable path for implementing acoustic streaming in conventional EWD platforms for enhanced mixing in LoC applications. At the cost of a modest increase in fabrication and operational complexity, our approach offers an acoustically active EWD top plate applicable to a general digital microfluidics platform. The novelty of the design presented here lies in the use of a thin, flexible polyester film for coupling acoustic energy directly into droplets held on independently driven EWD devices. Key advantages of our approach over other methods for piezoelectric integration include a fabrication methodology that is decoupled from the EWD bottom plate and greater flexibility in transducer material and geometry.

2 Experimental methods

Intra-droplet acoustic streaming was demonstrated with the use of 1.8 μm diameter fluorescent polystyrene microspheres. The device configuration shown in Fig. 1a illustrates the approach used to deliver out-of-plane ultrasound excitation to an underlying droplet held in place by an EWD actuator. Two key features differentiate the PZT/EWD device configuration from an otherwise standard parallel-plate EWD device. First, a PZT disk transducer is inserted into a through-hole machined into the EWD top plate. Second, a 127 μm Mylar coupling film is used to planarize the through-hole that accommodates the PZT disk. Figure 1a shows the PZT/EWD device schematic, while Fig. 1b shows a completely assembled test device. Figure 1c shows the hydrodynamic and acoustic streaming flow fields expected in the absence (left) and presence (right) of ultrasound excitation applied to the PZT transducer.

EWD devices were equipped with top plates that included a single embedded ultrasonic PZT transducer. Once fabricated, the PZT/EWD devices were staged in an inverted fluorescence microscope and operated under programmatic control. Droplets containing fluorescent microspheres were dispensed and transported to the center of the PZT transducer. Once in place, the droplets were exposed to controlled bursts of 250 kHz ultrasound, the resonant frequency of the PZT transducer. Ultrasound bursts consisted of 500 cycles each and were applied with a pulse repetition frequency

(PRF) of 50 Hz. The amplitude of the ultrasonic excitation was varied from 0 to 50 V_{RMS}, while fluorescence microphotographs were captured at 10 frames per second (fps). Microparticle image velocimetry (μPIV) was conducted to quantify hydrodynamic and acoustic streaming observed in the droplets. The following sections outline experimental details of the device fabrication, acoustics, optics, fluidics, and data analysis methods applied.

2.1 Design considerations

Several factors were taken into consideration in the choice of ultrasound frequency. First, previous analyses suggest good coupling and no deconstructive interference effects at an excitation frequency of 250 kHz (Madison 2015). Second, the ratio of acoustic radiation to streaming velocities, as computed by Barnkob et al. (2012), for 1.8 μm polystyrene microparticles in water exposed and to 250 kHz perturbation is expected to be ~ 0.3 . This suggests that at 250 kHz, acoustic streaming flow should dominate over radiation forces and result in circulating flow rather than the acoustophoretic concentration of particles at field nodes present in the droplet during insonation. Third, Landau and Lifshitz report that acoustic streaming is particularly pronounced under the condition: $\lambda \gg h \gg \delta_v$, where λ is the acoustic wavelength, h is the characteristic height of the microfluidic channel, and δ_v is the viscous penetration depth for an oscillating flow, which is given by (Landau and Lifshitz 2006):

$$\delta_v = \sqrt{\frac{2\mu}{\rho_0 \omega}}. \tag{5}$$

A frequency of 250 kHz applied to an aqueous droplet in a microfluidic channel of height, $h = 175\,\mu\text{m}$, ensures that the Landau–Lifshitz condition is met as $\lambda = c_0 \cdot f^{-1} \sim 6\,\text{mm}$ and $\delta_v = 1.1\mu\text{m}$, where c_0 is the speed of sound in water, 1495 $\text{m} \cdot \text{s}^{-1}$. These considerations suggest that the a resonant PZT frequency of 250 kHz will support acoustic streaming in the EWD device and that any induced fluid flow observed may be characterized by neutral-density tracer particles whose motion will couple to the acoustic streaming flow via the Stokes drag relation:

$$\mathbf{F}_\text{d} = 6\pi\mu a_\text{p}\left(\mathbf{v}_\text{p} - \langle \mathbf{v}_2 \rangle\right), \tag{6}$$

where a_p is the radius of the suspended particles.

2.2 Fabrication

Conventional EWD microfabrication methods were used to batch-produce EWD bottom plates as previously described (Madison 2015; Madison et al. 2016). We made one critical modification to an otherwise typical fabrication process to integrate a piston-shaped PZT transducer with EWD top plate. A transducer pocket was formed by milling a through-hole into the polycarbonate (PC) top plate substrate with a computer numeric control (CNC) end mill (Roland Modela MDX-20) and subsequently applying an adhesive-backed Mylar polyester (Grafix Plastics, Inc.) film to planarize the top plate. The planarizing film is a critical element that provides multiple functions in the PZT/EWD device including a mounting substrate for the PZT transducer, a smooth, flat surface, the EWD ground electrode, and a flexible acoustic coupling to the fluid layer.

A piston-shaped PZT transducer measuring 5 mm in diameter by 7 mm in height (APC International, Ltd.) was inserted into the transducer pocket, and a backing machined out of PC to accommodate the PZT disk was fixed to the top sides of the transducer face and the top plate with Loctite cyanoacrylate glue (Hankel Corp.). Strain relief was provided to the electrical leads of the PZT by securing a loop of the electrical leads to the transducer backing with 2 mil, 1/2" wide Kapton polyimide tape (McMaster-Carr). Additional detail on the fabrication procedure developed for integrating the PZT transducer with an EWD top plate is included in the Electronic Supplementary Material (ESM).

2.3 Acoustics instrumentation

Signal generation, amplification, and impedance matching instrumentation were required to produce controlled bursts with a 250 kHz ultrasound excitation applied to the PZT transducer in the PZT/EWD top plate. A waveform generator, programmed to output 5 V square pulses with a pulse repetition frequency (PRF) of 50 Hz, was used to trigger a second waveform generator, which was programmed to output 500 cycles of the 250 kHz sine wave of variable amplitude (0–250 $\text{mV}_\text{p-p}$), centered at 0 V. This 250 kHz signal was then amplified with a 55 dB RF amplifier to produce the signal applied to the PZT element, which ranged from 0 to 50 V_{RMS}. Impedance matching was found to be critical to the acoustic induction of fluid flow. Accordingly, we used an impedance matching transformer (Model JT-2-2-13, Electronics & Innovation, Ltd.) to match the impedance of the PZT transducer to that of the RF amplifier to more efficiently drive the PZT transducer. Additional detail on the acoustics instrumentation utilized for driving the PZT transducer is included in the ESM.

2.4 Inverted fluorescence microscopy

Inverted fluorescence microscopy was used to observe all electrowetting and acoustic streaming experiments. Yellow-green 1.8 μm fluorescent beads (Fluoresbrite YG Microspheres, Polysciences, Inc.) were used as neutral-density tracer particles to quantify the flow fields induced through

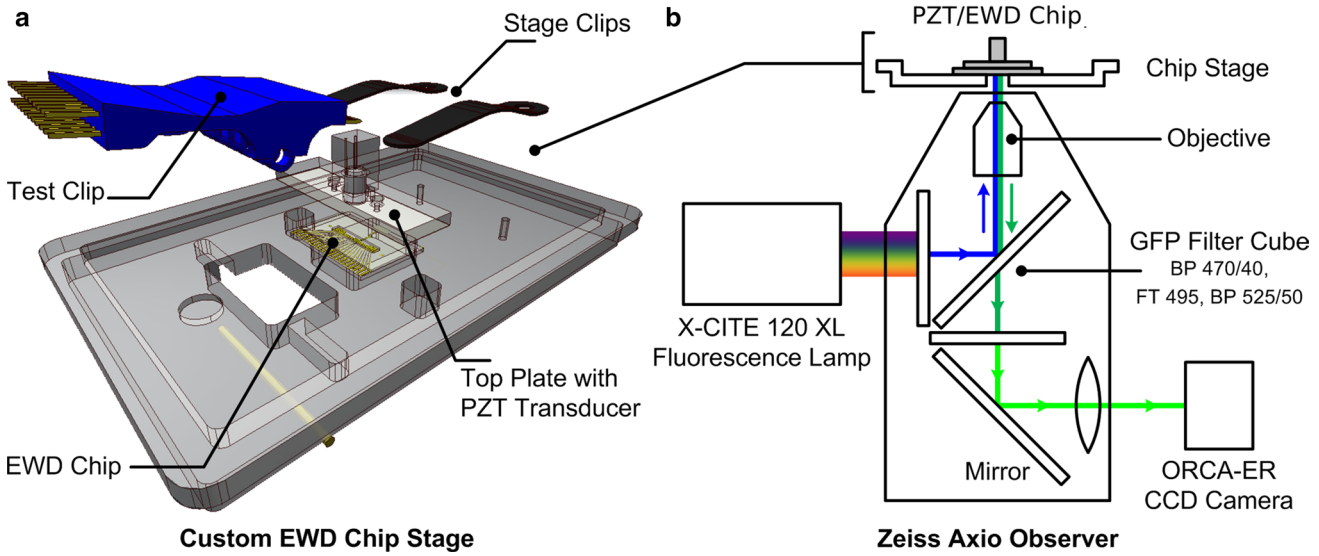

Fig. 2 Inverted fluorescence microscopy for flow field visualization. **a** Schematic of the microscope stage used for testing the PZT/EWD device; **b** optical system used to record μPIV measurements

EWD-based droplet immobilization and the application of ultrasound acoustic energy to a droplet held on an EWD actuator.

To accurately observe particle fluorescence, a custom PZT/EWD chip stage was machined to accommodate the inverted fluorescence microscope (Axio Observer, Zeiss). A drawing of the PZT/EWD chip stage is shown in Fig. 2a. Key features of the chip stage design include: the stage form factor, which matches that of the insert slot for the motorized stage of the microscope; a pocket for mounting the spring-loaded SOIC test clip and stage clips used for mechanically holding the top and bottom plates of the EWD system together; and an observation window beneath the mounting cite of the EWD chip for close proximity placement of a microscope objective. A schematic of the optical system used for μPIV in the PZT/EWD device is illustrated in Fig. 2b.

2.5 Fluidic manipulation and acoustic excitation

With the PZT/EWD test platform test apparatus assembled into an ultrasound-ready inverted fluorescence microscope arrangement, fluids were loaded onto the device where 200-nL droplets of aqueous suspensions of fluorescent microspheres were dispensed, immobilized under the PZT transducer, and exposed to 250 kHz ultrasound during observation.

Approximately 25 μL of 2 cSt silicone oil (Advanced Liquid Logic, Inc.) was added to the EWD devices via the pipette inlets near the fluid reservoirs. A basic EWD apparatus was used for all DMF droplet actuation, as previously described (Madison et al. 2016). The electrowetting waveform was set to a 1 kHz, 35 $V_{p\text{-}p}$ (12.4 V_{RMS}) sine wave, and an EWD control graphical user interface[1] (GUI) was used to energize the reservoir electrodes on one side of the PZT/EWD device. A dilute suspension of YG microspheres was prepared by pipetting 0.5 μL of the stock suspension into 1 mL of 0.05% Tween-20 in a 1.5-mL microcentrifuge tube, producing a final concentration of 2.8×10^6 particles $\cdot mL^{-1}$. With the EWD reservoir electrodes activated, 2 μL of the diluted suspension of YG microspheres was pipetted into one EWD reservoir.

Once the EWD reservoirs were loaded with the YG microsphere suspension, single droplets were dispensed and actuated to the electrode centered beneath the PZT transducer. Droplets were then exposed to 500 bursts of 250 kHz ultrasound while being held in place by a single EWD electrode energized with a 1 kHz, 35 $V_{p\text{-}p}$ (12.4 V_{RMS}) sine wave. Each acoustic burst consisted of 500 cycles of a 250 kHz sine wave repeated at 50 Hz for a total ultrasound exposure of 1 s applied over 10 s. The preamplified ultrasound signal was varied from 0 to 250 $mV_{p\text{-}p}$. After amplification through a 55 dB RF amplifier, the amplitude ranged from 0 to 50 V_{RMS} as verified with an oscilloscope (Model 54624A, Agilent Technologies) and 1:100 probe.

2.6 Data acquisition and analysis

Sequences of fluorescence micrographs, recorded at a wavelength of $\lambda = 525 \pm 25$ nm, were acquired at a frame rate of 10 fps before, during, and after exposure using MetaMorph®

[1] The EWD control GUI software is available upon request.

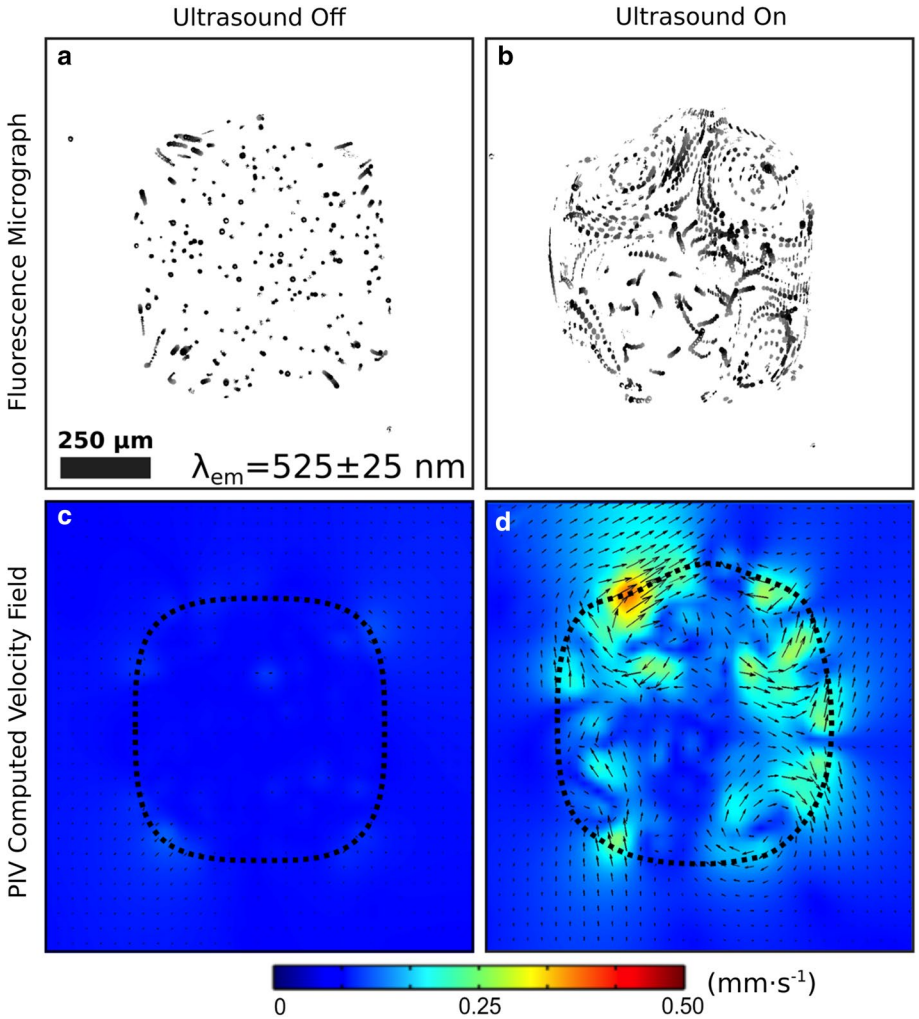

Fig. 3 Fluorescence micrographs and µPIV results. An overlay of 8 fluorescence micrographs of a single 200 nL droplet of 1.8 µm particles immobilized on an EWD electrode reveals the particle trajectories observed for 1 s in the absence (**a**) and presence (**b**) of ultrasound excitation; grayscale intensity indicates relative time measure where light gray pixels correspond to $t = t_0 - 1$ s and black to $t = t_0$. Computed velocity fields in the absence (**c**) and presence (**d**) of the ultrasound excitation; the droplet interface is indicated by the dotted line. A time series of raw fluorescence micrographs and processed frames resulting from the µPIV are shown in two movies included in the ESM (color figure online)

microscopy automation and image analysis software. Exposure times of 20 ms were used for each micrograph taken in each 200-image (20 s) sequence. The resulting image stack was analyzed using the open-source µPIV suite PIVlab v.1.4 in MATLAB® to quantify induced particle velocities for the range of excitation amplitudes incident on the PZT transducer (Thielicke and Stamhuis 2014).

3 Results and discussion

The application of 250 kHz ultrasound to a single, EWD-immobilized droplet of 1.8 µm polystyrene microspheres was found to reproducibly induce fluid flow within EWD-immobilized droplets. Streaming velocities as high as 2.5 $mm \cdot s^{-1}$ were observed in flow fields that did not breach the droplet interface. Induced velocity distributions were well approximated by a gamma distribution with a median value proportional to the square of the excitation voltage.

An overlay of 8 fluorescence micrographs captured in the absence (a) and presence (b) of a 30 V_{RMS} excitation to the droplet is shown in Fig. 3. Corresponding magnitudes of the velocity fields computed with µPIV before and during the application of a 30 V_{RMS} excitation are shown in Fig. 3c and d, respectively. Figure 3a and c depicts the hydrodynamic flow in a droplet under oscillating electrowetting bias only, while Fig. 3b and d shows the droplet during exposure to the 250 kHz perturbation. A comparison of Fig. 3a and c to b and d qualitatively reveals the occurrence of acoustic streaming activity. Moreover, the particle trajectories observed for 1 s of ultrasound exposure shown in Fig. 3b indicate the presence of several closed circulation paths that arise throughout the extents of the droplet. Conversely, particle trajectories observed for a similar period in the absence of ultrasound excitation are much more subdued, appearing primarily in the corners of the immobilized droplet where regions of greater curvature drive hydrodynamic flow. Further, the magnitude of the velocity field, as visualized by shaded surface with vector arrows, is significantly greater

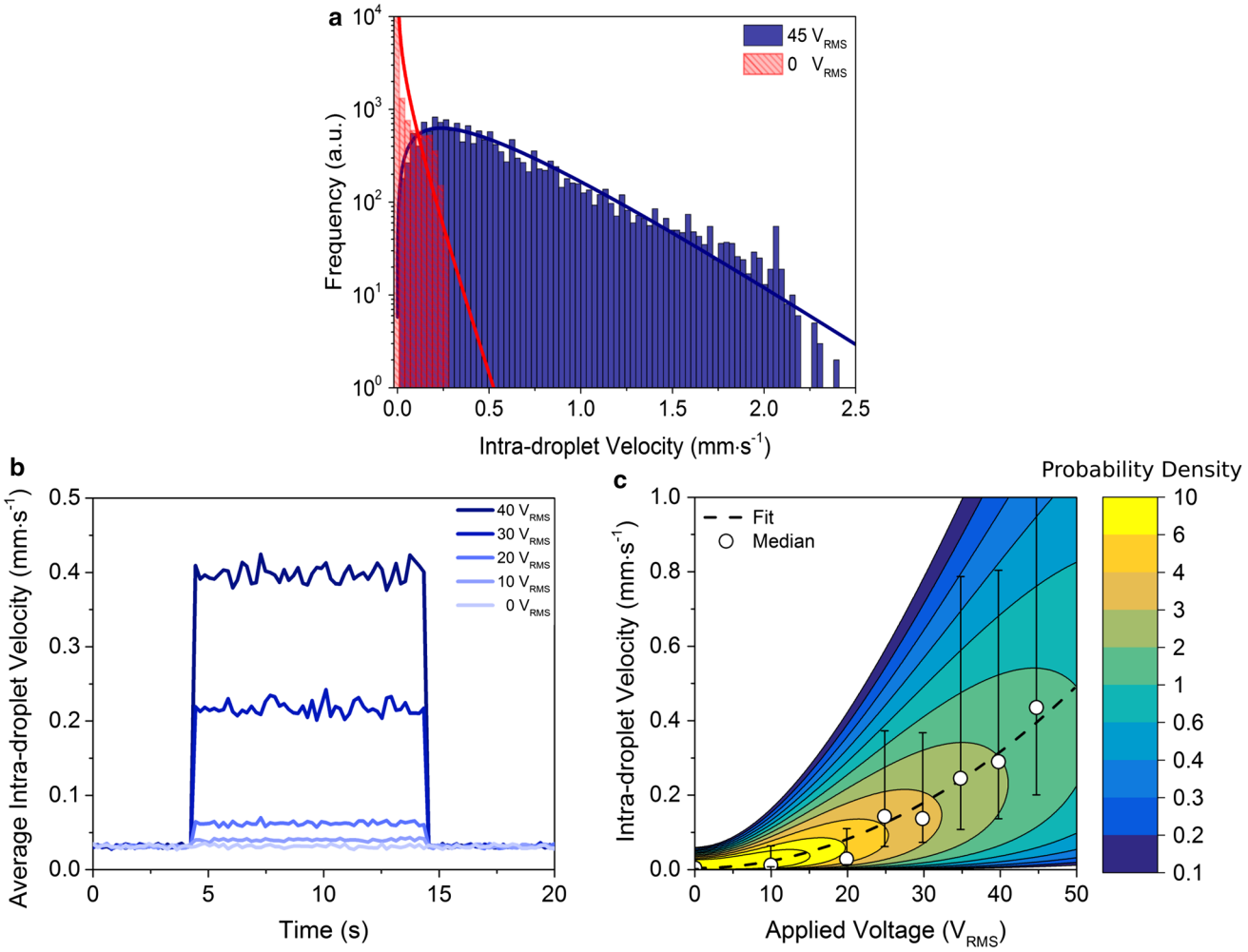

Fig. 4 Quantification of intra-droplet acoustic streaming flows. **a** Distribution of intra-droplet fluid velocity in the absence of acoustic excitation, *i.e.*, under oscillating electrowetting bias only (red) and in the presence of 45 V_{RMS} acoustic excitation (blue); solid bars indicate μPIV measurements, while the respective lines indicate fits to a gamma distribution. **b** Time series plot of average intra-droplet velocity for 0, 10, 20, 30, and 40 V_{RMS} throughout the full 10 s exposure schema. **c** Distribution, median, and quartiles of the acoustic streaming flows observed for a range of excitation voltages applied to the PZT transducer (color figure online)

in Fig. 3d than in c. Second, the vector plot reveals the presence of fluid flow that comprises multiple circulating regions within the exposed droplet. Lastly, the droplet interface shows slight deformation in response to inertial forces present in the streaming field, which was characterized by a median and maximum fluid velocities of 0.13 and 0.37 $mm \cdot s^{-1}$, respectively.

Fluorescence micrographs similar to those shown in Fig. 3 were captured at 10 fps throughout the entire 20 s ultrasound exposure for each excitation voltage applied to the PZT transducer. Intra-droplet microstreaming velocity profiles were computed, and descriptive statistics of the microstreaming velocity were calculated for the intra-droplet region. This analysis produced time-correlated histograms of the fluid velocity field within the droplets for each excitation amplitude. Figure 4a shows distributions the intra-droplet velocity magnitudes in the absence (red) and presence (blue) of a 45 V_{RMS} 250 kHz excitation. The baseline fluid velocity of 0.032 ± 0.057 $mm \cdot s^{-1}$, which was observed during PZT quiescence, indicates hydrodynamic flow due to the 1 kHz oscillating EWD actuation bias. In contrast, an induced streaming velocity of 0.554 ± 0.430 $mm \cdot s^{-1}$ was measured at a PZT driving voltage of 45 V_{RMS} indicating significant acoustic streaming activity at 250 kHz.

Time-correlated statistics of the velocity magnitude reveal a striking contrast in control of intra-droplet fluid flow for the experimental range of input ultrasound amplitudes. Figure 4b shows a time series plot of the average intra-droplet velocity for the experimental range of excitation potentials applied to the PZT transducer. Note the abrupt change in average velocity magnitude that occured when the

ultrasound excitation was asserted and deasserted. The data clearly indicate a rapid increase in average fluid velocity that scales with excitation amplitude.

Trends observed in median intra-droplet fluid velocity magnitude suggest a quadratic relationship between the applied excitation potential, V_{RMS}, and the acoustic streaming field, $\langle \mathbf{v}_2 \rangle$. Figure 4c shows a plot of the median of the intra-droplet velocity magnitude (white circles) with error bars indicating the upper and lower quartiles of the distribution as measured by μPIV. Nonlinear curve fitting was used to elucidate the coefficients of the quadratic relationship between median fluid velocity magnitude, v_{md}, and excitation amplitude to be: $a = 1.898 \times 10^{-4}\ \mathrm{mm \cdot s^{-1} \cdot V^{-2}}$ and $c = 0.012\ \mathrm{mm \cdot s^{-1}}$ with $R^2 = 0.949$ for the parabolic fit function, $v_{\mathrm{md}} = aV_{\mathrm{RMS}}^2 + c$.

In addition to the quadratic dependence on PZT driving voltage, the data also indicate that the spread in the intra-droplet velocity distribution increased with the PZT driving voltage. The intra-droplet velocity distribution was found to be well approximated by the gamma distribution function, f_Γ with a mean value, $\bar{v}$, proportional to the amplitude of ultrasound excitation squared, as shown in Eq. 7

$$f_\Gamma = \frac{1}{\Gamma(\alpha)\beta^{-\alpha}} v^{\alpha-1} \mathrm{e}^{-v\beta}, \tag{7}$$

where $\alpha = 2$, $\Gamma(\alpha) = \int_0^\infty v^{\alpha-1}\mathrm{e}^{-v}\mathrm{d}v$, and $\bar{v} = \frac{\alpha}{\beta} = 2.72 \times 10^{-4} V_{\mathrm{RMS}}^2 + 0.013\,(R^2 = 0.948)$. To illustrate this trend, log-spaced contours of the gamma distribution probability density for a quadratically increasing mean in intra-droplet velocity magnitude are plotted as a shaded surface beneath the median of the intra-droplet velocity magnitude.

3.1 Droplet breakup

Droplet excitation was found to be unstable for excitation voltages in excess of $\sim 50\ \mathrm{V_{RMS}}$. Rapid droplet breakup and ejection from the EWD actuator were repeatedly observed at elevated excitation amplitudes of the PZT transducer. The absorption of momentum from the incident acoustic wave may drive the droplet interface with greater force than the electrowetting force used to immobilize the excited droplet. We define the EWD stabilization number, $\mathrm{St_{EWD}}$, as the ratio of the electrowetting number, η, to the Weber number, We. In the present case, $\mathrm{St_{EWD}}$ represents effects of the electrowetting force acting at the droplet contact line relative to induced inertial forces from the acoustic streaming field:

$$\mathrm{St_{EWD}} = \frac{\eta}{\mathrm{We}} = \frac{\varepsilon_0 \varepsilon_\mathrm{r} V^2}{2d\rho U^2 l}, \tag{8}$$

where V is the root-mean-square of the EWD voltage, U is the magnitude of the induced fluid velocity, and l is the droplet diameter. The fluidic and electrowetting parameters employed in our experiments, $d = 2\,\mu\mathrm{m}$, $\rho = 1000\ \mathrm{kg \cdot m^{-3}}$, $l = 700\,\mu\mathrm{m}$, $\varepsilon = 2.9$, and $V = 12.4\,V_{\mathrm{RMS}}$, suggest that inertial forces from the acoustic streaming activity balance with the electrowetting forces at a critical streaming velocity magnitude of $\|\langle \mathbf{v}_2 \rangle\| = 22\ \mathrm{mm \cdot s^{-1}}$, which is within an order of magnitude of the maximum streaming velocity measured for PZT driving voltages around $50\ \mathrm{V_{RMS}}$. Hence, it is feasible that high-amplitude ultrasonic excitation may drive streaming fields that simply overpower the electrowetting holding force leading to interfacial instability and ultimately droplet dispersion from the EWD electrode.

4 Conclusion

Acoustic streaming activity was demonstrated within 200 nL droplets immobilized on an EWD electrode. Pulsed ultrasound excitation of 250 kHz and variable amplitude was used to generate circulating fluid motion of controllable velocity magnitude within droplets held in place on single electrodes. During ultrasound exposure, particle image velocimetry revealed streaming velocities as high as $2.5\ \mathrm{mm \cdot s^{-1}}$ for aqueous droplets containing suspensions of 1.8 μm fluorescent beads. The velocity distributions measured during ultrasound exposure were well approximated by a gamma distribution function with a mean value that scaled quadratically with the PZT excitation voltage. One limitation of the method was observed at high PZT excitation amplitudes where droplet dispersion occured. Droplet dispersion and, ultimately, breakup of immobilized droplets exposed to high-amplitude ultrasonic perturbation illustrate the competing action between the EWD holding force and the induced acoustic streaming activity generated within and around the droplet.

Controllable piezo-driven acoustic streaming, as demonstrated in this work, provides a viable path toward implementing active micromixing in a EWD platform with a straightforward modification to the top plate geometry. The combination of through-hole geometry and thin planarizing film was sufficient for establishing a mechanical coupling between a compact PZT transducer and an underlying discretized fluid layer. This simple arrangement opens up the possibilities for exploring the utility of ultrasound applications in the EWD environment by obviating the need for advanced piezoelectric materials fabrication.

Acknowledgements The authors thank the staff of Duke University's Shared Materials Instrumentation Facility (SMiF) for fabrication support, Dr. Yasheng Gao of the Light Microscopy Core Facility (LCMF)

of Duke University for microscopy assistance, and Dr. Laura B. Lewandowski for editorial support.

Compliance with ethical standards

Conflict of interest The authors declare no conflicts of interest.

References

Ahmed D, Mao X, Shi J, Juluri BK, Huang TJ (2009) A millisecond micromixer via single-bubble-based acoustic streaming. Lab Chip 9:2738–2741

Alghane M, Fu YQ, Chen X, Li Y, Desmulliez MPY, Walton AJ (2012) Frequency effect on streaming phenomenon induced by rayleigh surface acoustic wave in microdroplets. J Appl Phys 112(084902):1–12

Baret JC, Decré MM, Mugele F (2007) Self-excited drop oscillations in electrowetting. Langmuir 9:5173–5179

Barnkob R, Augustsson P, Laurell T, Bruus H (2012) Acoustic radiation- and streaming-induced microparticle velocities determined by microparticle image velocimetry in an ultrasound symmetry plane. Phys Rev E 86(056307):1–11

Berge B (1993) Electrocapillarity and wetting of insulator films by water. Comptes rendus de l'Acadèmie des Sciences, Séries II(317):157–163

Bruus H (2011) Acoustofluidics 1: governing equations in microfluidics. Lab Chip 11:3724–3751

Bruus H (2012) Acoustofluidics 2: perturbation theory and ultrasound resonance modes. Lab Chip 12:20–28

Eckart C (1948) Vortices and streams caused by sound waves. Phys Rev 73:68–76

ePlex® (2016) Sample-to-answer multiplex molecular diagnostics. Brochure. https://www.genmarkdx.com/wp-content/uploads/2016/07/GNMK-IMC-1039-B-ePlex-4-page-Brochure.pdf

Huang PH, Xie Y, Ahmed D, Rufo J, Nama N, Chen Y, Chan CY, Huang TJ (2013) An acoustofluidic micromixer based on oscillating sidewall sharp-edges. Lab Chip 13:3847–3852

Illumina® Neoprep™ library prep system (2016) Specification sheet: sequencing. http://www.illumina.com/content/dam/illumina-marketing/documents/products/datasheets/neoprep-system-datasheet-970-2014-004.pdf

Ko SH, Lee H, Kwan HK (2008) Hydrodynamic flows in electrowetting. Langmuir 24:1094–1101

Landau LD, Lifshitz EM (2006) Fluid mechanics. Volume 6 (course of theoretical physics), Second Edition. Butterworth-Heinemann, Amsterdam

Lee CP, Chen HC, Lai MF (2012) Electrowetting on dielectric driven droplet resonance and mixing enhancement in parallel-plate configuration. Biomicrofluidics 6(1):012814–012814-8

Li Y, Fu YQ, Brodie SD, Alghane M, Walton AJ (2012) Integrated microfluidics system using surface acoustic wave and electrowetting on dielectrics technology. Biomicrofluidics 175(012812):1–9

Lippmann G (1875) Relations entre les phénomènes électriques et capillaires. Ann Rev Chim Phys 5:494

Liu RH, Yang J, Pindera MZ, Athavale M, Grodzinski P (2002) Bubble-induced acoustic micromixing. Lab Chip 2:151–157

Lu HW, Bottausci F, Fowler JD, Bertozzi AL, Meinhart C, Kim CJ (2008) A study of EWOD-driven droplets by PIV investigation. Lab Chip 8:456–461

Luong TD, Phan VN, Nguyen NT (2011) High-throughput micromixers based on acoustic streaming induced by surface acoustic wave. Microfluid Nanofluid 10:619–625

Madison AC (2015) Scalable genome engineering in electrowetting on dielectric digital microfluidic systems. Ph.D. thesis, Duke University, Durham, NC 27708, USA. http://search.proquest.com/docview/1718503132

Madison AC, Royal MW, Fair RB (2016) Fluid transport in partially shielded electrowetting on dielectric digital microfluidic devices. J Microelectromech Syst 25(4):593–605. https://doi.org/10.1109/JMEMS.2016.2561699

Mugele F (2009) Fundamental challenges in electrowetting: from equilibrium shapes to contact angle saturation and drop dynamics. Soft Matter 5:3377–3384

Mugele F, Baret JC, Steinhauser D (2006) Microfluidic mixing through electrowetting-induced droplet oscillations. Appl Phys Lett 88(204):106

Muller PB, Barnkob R, Jensen M, Bruus H (2012) A numerical study of microparticle acoustophoresis driven by acoustic radiation forces and streaming-induced drag forces. Lab Chip 12:4617–4627

Pollack MG, Shenderov AD, Fair RB (2002) Electrowetting-based actuation of droplets for integrated microfluidics. Lab Chip 2:96–101

Rayleigh L (1884) On the circulation of air observed in Kundt's tubes, and on some allied acoustical problems. Philos Trans R Soc Lond 175:1–21

Riley N (2001) Steady streaming. Ann Rev Fluid Mech 33:43–65

Shilton R, Tan MJ, Yeo LY, Friend JR (2008) Particle concentration and mixing in microdrops driven by focused surface acoustic waves. J Appl Phys 104(014910):1–9

Thielicke W, Stamhuis EJ (2014) PIVlab—towards user-friendly, affordable and accurate digital particle image velocimetry in MATLAB. J Open Res Softw 2(1):30

Wiklund M, Green R, Ohlin M (2012) Acoustofluidics 14: applications of acoustic streaming in microfluidic devices. Lab Chip 12:2438–2451